Promoting Structural and Anticorrosive Performances via Accumulative Roll Bonding to a Ti-Ta-Nb Alloy

D. Raducanu[1], C. Vasilescu[2], A. Nocivin[3], S. I. Drob[2,], I. Cinca[1], D. Gordin[4] M. Marcu[2] and V. D. Cojocaru[1]*

[1] Polytechnic University of Bucharest, Faculty of Materials science and Engineering, Spl. Independentei 313, 060042 Bucharest, Romania
[2] Institute of Physical Chemistry "Ilie Murgulescu" of Romanian Academy, Spl. Independentei 202, 060021, Bucharest, Romania.
[3] Ovidius University of Constanta, Faculty of Mechanical, Industrial and Maritime Engineering, 124 Mamaia Ave., 900527, Constanta, Romania
[4] INSA de Rennes, Laboratoire Chimie-Métallurgie, UMR CNRS 6226 Institut des Sciences Chimiques de Rennes, 20 avenue des Buttes de Coësmes, 35708 Rennes Cedex 7, France
*E-mail: sidrob@chimfiz.icf.ro

Present work has as objective to demonstrate the positive increase of the corrosion resistance through particular Ultra-Fine Grained (UFG) or Nano Crystalline (NC) structures obtained by Severe Plastic Deformation (SPD) on recently new developed β-type Ti-25Ta-25Nb alloy. The alloy was processed by Accumulative Roll Bonding (ARB) method, applying four ARB cycles at ambient temperature. The micro-structural characterization was performed before and after each ARB cycle, using XRD and SEM analysis. For all four structural states corresponding to ARB processed alloy (with 2, 4, 8 and respectively 16 layers), has been determined the phase quantities for both detected β-Ti and α"-Ti phases, the lattice parameters values for each crystalline system of the present phases, and the average coherent crystalline domain size. The SEM analysis highlights the nano-grained character of the structure obtained gradually by increasing the number of ARB cycles. Corrosion potentials are nobler and ennobled with the number of ARB cycles due to the favorable effect of the ARB processing; values of the corrosion current densities and of the corrosion rates are lower for ARB processed alloy than that of as-cast alloy and decrease with the increase of the number of layers confirming a more protective passive film; polarization resistances have higher values for ARB processed alloy, namely, a better passivity. Values of the Tafel slopes show the anodic control of the corrosion process at the interface between alloy and simulated physiological fluid. All these facts suggest the improvement of protective properties of the passive oxide layer, existing on the processed alloy surface. All corrosion parameters enhanced their values by the increase of the layer stacks, namely, the ARB processing has a positive influence on the alloy corrosion resistance. The increase of the number of ARB cycles conducted to the thickening and stability in time of the alloy passive film.

1. INTRODUCTION

Highly biocompatible β-Ti based alloys [1, 2] represent a class of alloys situated at maximum attention of researcher groups for the last decade, being excellent candidates for medical applications, because of their performing mechanical properties [3-5] such as high strength to density ratio, high mechanical resistance and low elastic modulus closer to that of natural bone, but most of all because of their superior biocompatibility and high corrosion resistance [6-8] capable to avoid the release of ions and corrosion products in the surrounding tissues that can ultimately affect their biocompatibility [9-11]. The advantage of the body centered cubic (bcc) β phase is that it is more ductile than the hexagonal compact (hc) α phase, and therefore can be more easily ultra-grain refined until nano-crystalline level, which can improve the alloy bioactivity and mechanical performances compared with their coarse grained counterparts [4, 12-16]. In this context, the present work has as objective to demonstrate the positive achievements like highly corrosion resistance through particular Ultra-Fine Grained (UFG) or Nano Crystalline (NC) structures obtained by Severe Plastic Deformation (SPD) on recently new developed β-type Ti-25Ta-25Nb alloy. This alloy is of great interest for biomedical applications due to a very good combination of properties, proved by several recent investigations [8, 17-20], but referring only to equiaxed homogeneous coarse grain microstructure and not to UFG/NC structural state. It's already known that non-toxic niobium and tantalum, like alloying elements in β-Ti alloys, exhibit an increasing of the corrosion resistance and biocompatibility of the biomaterial, Ta being more corrosion resistant than Nb due to higher stability of its oxide [2, 3, 9]. Thus, it remains to ascertain good corrosion resistance of UFG/NC structural state for selected alloy, which can be obtained by severe plastic deformation. One of the most applied and successful method of producing UFG/NC materials in bulk dimensions by SPD is accumulative roll-bonding (ARB) [21-24]. The formation mechanism of UFG/NC structure during ARB processing can be explained in terms of grain subdivision at submicron scale [21-24] where initial coarse-grains have been subdivided by deformation-induced in high-angle grain boundaries [24]. The ARB process involves severe plastic deformation of the alloy by rolling two equally geometrical dimensioned stacked material sheets, with a deformation degree of 50%. In these conditions, the final consolidated stacked sheet will have a final thickness equal to that of each original sheet before rolling. The ARB process can be applied for unlimited plastic deformations and for unlimited number of ARB cycles. The grain dimensions decrease after each ARB cycle, until UFG or even NC dimensions are achieved. The intention of this work is to prove superior structural and anticorrosive performances of this alloy in UFG/NC structural state, obtained by ARB process, compared with common coarse grained structure.

2. EXPERIMENTAL PART

2.1. Alloy synthesis, thermo-mechanical processing, ARB processing

The selected alloy Ti-25Ta-25Nb (wt.%) has been synthesized from commercially pure elements, using a levitation induction melting furnace FIVE CELES - MP25 with nominal power 25

kW and melting capacity 30 cm^3, under argon protective atmosphere. The final chemical composition had no more than 0.1 wt. % compositional variations from that initial proposed, which therefore have been considered to be negligible. This applied alloy synthesis method is efficient for melting metals with big difference between melting points, in order to obtain ingots with high chemical homogeneity, without risk of contamination. For the present case, the large difference in melting temperatures (Ti: 1660°C; Ta: 2996°C; Nb: 2468°C) has required two times re-melting of the obtained ingots, in order to realize a high chemical homogeneity. After that, the Ti-25Ta-25Nb alloy was processed by a complex thermo-mechanical (TM) processing route (Fig. 1), in order to provide a thin precursor strip necessary for obtaining, by accumulative roll-bonding (ARB), of multi-layered stacked strips, consisting of 2, 4, 8 and 16 layers stacks.

The TM process comprises the following steps: first - a cold-rolling (CR I) with a thickness reduction of about 85.83% (equivalent strain ε = 1.85) for a 20 rolling passes, followed by a recrystallization treatment in protective atmosphere of argon, at 850°C / 30 min / air cooling, using a GERO SR 100x500 heat treatment oven. The recrystallization treatment was performed in order to remove the strain-hardening effects resulted during first cold-rolling. After recrystallization, a second cold-rolling (CR II) was applied, with a thickness reduction of about 67.97% (equivalent strain ε = 1.24) for 8 rolling passes, in order to achieve 141 μm final strips thickness. This final strip represents the ARB precursor layer. The ARB process itself consisted in four ARB passes in order to obtain 2, 4, 8 and 16 layers stacks. Both cold-rolling processes (CR I and CR II) and the ARB passes were carried out using a Mario di Maio LQR120AS rolling-mill, at 3 m/min rolling speed, without any lubrication. Before ARB process, the TM processed samples were cleaned in an ultrasonic bath at temperature of 60ºC, in ethylic alcohol.
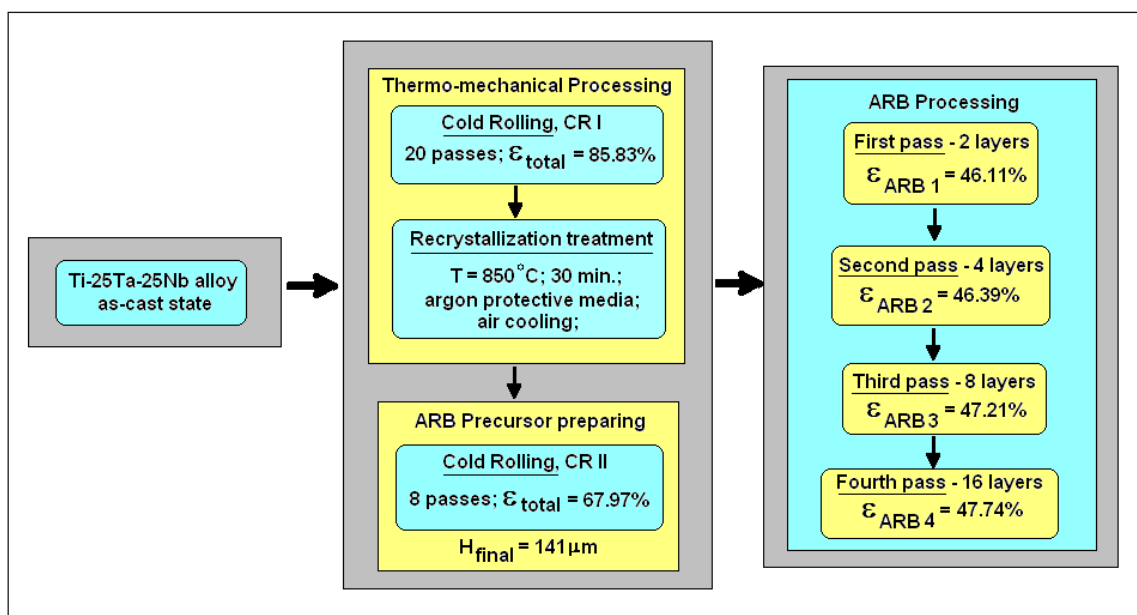

Figure 1. Thermo-mechanical processing and accumulative roll bonding (ARB) of initial as-cast Ti-25Ta-25Nb alloy

2.2. Structural characterization of the alloy

To determine phase structure and phase characteristics of the alloy, the ARB precursor and ARB processed specimens (with 4 layers and 16 layers) were XRD characterized, using a Panalytical X'Pert PRO MRD diffractometer, with Cu k-alpha ($\lambda = 0.15418$ nm). The recorded XRD spectra were fitted by PeakFit v4.11 software package, in order to determine for each diffraction peak the position, intensity and peak broadening - FWHM (Full Width at Half Maximum) parameters.

For the micro-structural characterization of the precursor sample and ARB processed samples, the SEM analysis was performed using a scanning electron microscope TESCAN VEGA II – XMU.

The specimens were fixed on specific epoxy resin, abraded with 1200 grit SiC paper, and mechanically polished using 6, 3, 1 μm diamond paste and 0.03 μm colloidal silica. Total removed thickness of the layer was about 150 μm. For the samples subjected to cold-rolling, the observation plane was parallel to rolling direction, in the T-L plane.

2.3. Corrosion behavior in Ringer solution

The corrosion behavior [25] of Ti-25Ta-25Nb alloy in ARB processed states was studied in comparison with that of alloy in as-cast state by linear polarization measurements and time monitoring of the open circuit potentials in simulated physiological fluid, Ringer solution of composition (g/L): NaCl – 6.8; KCl – 0.4; $CaCl_2$ – 0.2; $MgSO_4.7H_2O$ – 0.2048; $NaH_2PO_4.H_2O$ – 0.1438; $NaHCO_3$ -1.1; glucose – 1; temperature was kept at $37^{o} \pm 1^{o}C$.

The samples cut from the alloy in as-cast and ARB processed state were ground with metallographic paper till 2000 granulations and then with 1 μm aluminum oxide to mirror surface. After that they were ultrasonically degreased in acetone and water for 15 min.

Linear polarization measurements were performed using Voltalab 80 equipment with VoltaMaster 4 program; the curves were registered for ±50 mV around the open circuit potential with a scan rate of 1 mV/s. From Tafel representations, the main corrosion parameters were determined: E_{corr} – corrosion potential, i_{corr} – corrosion current density; V_{corr} – corrosion rate; R_p – polarization resistance, β_a – anodic Tafel slope, β_c – cathodic Tafel slope [26-28].

The open circuit potentials (E_{oc}) were monitored for a time period of 1500 hours with a performing Hewlett-Packard multimeter. The time variations of these potentials were statistically analyzed with Medcalc program. It was determined the frequency and the distribution of E_{oc} values by histograms, the way of variation with the scatter diagrams and the regression curves. The relation E_{oc} – time was established by the regression equations that permit the calculation of the E_{oc} values for longer time periods than the experimental one; the credibility of these equations can be evaluated by determination coefficients, D (values from 0.8 to 1.0 provide a high credibility level of the prognosis).

All experiments were carried out on the three samples; reproducibility was very good and average value of the three measurements was considered.

3. RESULTS AND DISCUSSION

3.1. Structural characterization and analysis of the alloy

Like was defined in the introduction part, the intention of present work is to prove the superior qualities of Ti-25Ta-25Nb alloy in UFG/NC structural state, obtained by ARB process, compared with the common coarse grained structure of the precursor sample. All structural modifications which appear during ARB process are supposed to develop superior mechanical properties and also chemical properties such as biocompatibility. The structural modifications (changes in phase structure, phase quantities, lattice parameters and coherent crystalline domain size) during the ARB process can be described and analyzed using the XRD and SEM investigations.

Concerning the XRD experiments [29-31], there have been performed on as-cast state, ARB precursor, ARB 4 layers and ARB 16 layers states. Fig. 2 shows the XRD spectra for these investigated states. In all four different states can be observed the presence of β-Ti and α"-Ti phases. Table 1 indicates for all four structural states the lattice parameters values determined for each crystalline system of the present phases, the phase quantities for each case and the average coherent crystalline domain size for both β-Ti and α"-Ti phases (that were calculated using simple Scherer equation [32], taking into account specific phase diffraction lines - fitted position, intensity and peak broadening).
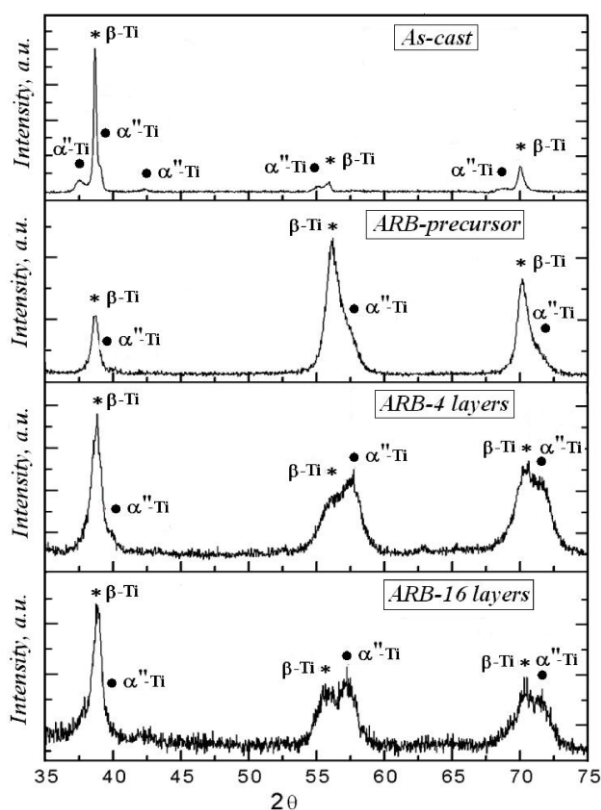

Figure 2. XRD spectra of Ti-25Ta-25Nb alloy in: as-cast state; ARB precursor state; ARB 4 layers processed state; ARB 16 layers processed state.

Analysing the XRD spectra and the calculated data from Table 1 it can be appreciated how the phase quantity evolution was during the ARB process, correlated with the corresponding values of the coherent crystalline domain size. Thus, while in as-cast sample the structure is formed by dominant β phase (99.52%) due to β stabilizing alloying elements – Nb and Ta, beginning with following stages, the α"-Ti phase began to increase quantitatively step by step, until 42.62% for the ARB-16 layers sample. This increase of α"-Ti phase is explained by the stress - induced phase transformation from the body centred cubic-bcc unstable β phase to the orthorhombicα"- martensite (β → α") which occurs during ARB process [19]. If compare the precursor sample with the ARB-16 layers sample, the α"-Ti phase increases from 6.21% to 42.62%, while the average of the coherent crystalline domain size decreases from 31 nm until 16 nm, which means a diminution with half dimension.

Table 1. Phase content, corresponding lattice parameters, phase quantity and the average of coherent crystalline domain size (CCDS) for each structural state of Ti-25Ta-25Nb alloy.

Structural state of the alloy	Phase content	Lattice parameters (nm)	Phase quantity (%)	CCDS (nm)
As-cast	β-Ti	a = 0.3288 BCC system - *Im-3m*	99.52±0.23	82
	α"-Ti	a = 0.31811 b = 0.4813 c = 0.4631 Orthorhombic system - *Cmcm*	0.48±0.11	14
ARB precursor (TM processed)	β-Ti	a = 0.3284	93.79±1.17	28
	α"-Ti	a = 0.3211 b = 0.4731 c = 0.4632	6.21±0.68	31
ARB 4 layers	β-Ti	Similar to precursor	61.19±2.84	24
	α"-Ti		38.81±3.09	21
ARB-16ayers	β-Ti	Similar to precursor	57.38±4.31	22
	α"-Ti		42.62±3.11	16

[a]The average of coherent crystalline domain size

This final nano-crystalline structure underlines the idea that ARB process is proper for ultra-fine graining of the structure correlated with the β-Ti/α"-Ti ratio decreasing which can be controlled in function of the final necessary mechanical properties of the alloy: if we are interested in the obtaining high material strength, then we need to steer the structure towards small coherent crystalline domains, but if we intend to obtain a desired elastic modulus, in a certain interval range, than we need to steer the structure towards a certain phase β-Ti/α"-Ti ratio (β-Ti phase exhibits a low elastic modulus while α"-Ti phase exhibits a higher elastic modulus). This variation of the structural particularities indicates that it is possible to steer the phase structure (phase quantities and coherent crystalline domain size) in order to obtain the desired final properties of the material.
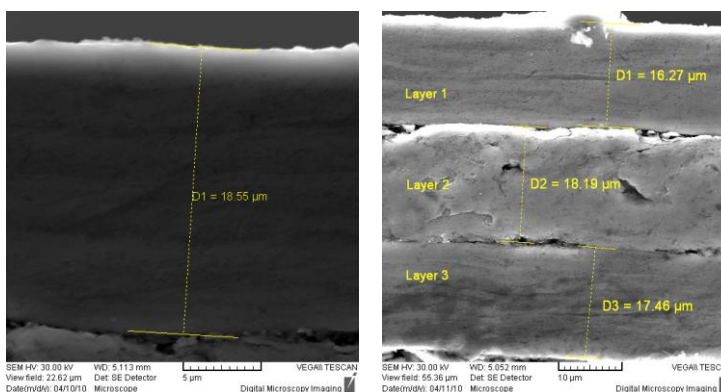
Figure 3. SEM images corresponding to ARB processed Ti-25Ta-25Nb alloy − 4 layers: a) detailed image of one layer, with corresponding thickness of D1=18.55 μm; b) image is focused only on three from all four layers.

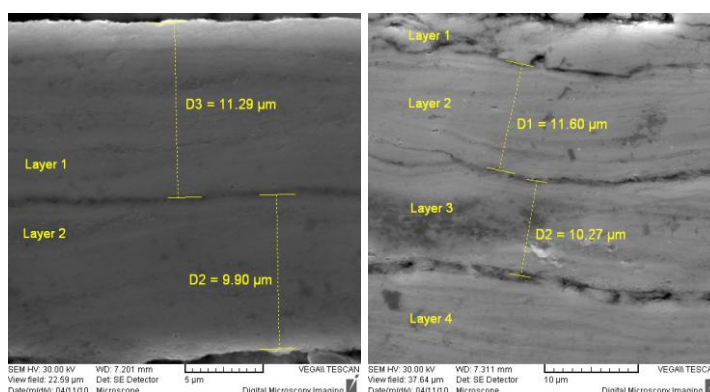**Figure 4.** SEM images corresponding to ARB processed Ti-25Ta-25Nb alloy − 8 layers: a) detailed image of two layers, with corresponding thickness of D2=9.90 μm and D3=11.29μm; b) image is focused only on four from all eight layers.
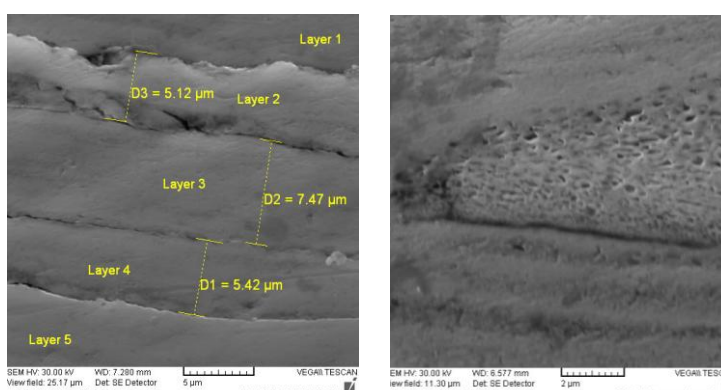

Figure 5. SEM images corresponding to ARB processed Ti-25Ta-25Nb alloy − 16 layers: a) image is focused only on five from all sixteen layers; b) detailed image of one layer.

Completing the structural analysis with SEM investigations [33], the Figs. 3-5 indicate the SEM microscopic aspects of the studied alloy during ARB process (4, 8 and 16 layers). A good

adhesion between the layers can be seen from SEM images. Also, it can be observed the decreasing of the layers thickness as the ARB process is developed, from about 17 μm (for ARB-4 layers sample – Fig. 3) to the smallest layer thickness of 5 μm (for ARM-16 layers sample – Fig. 5). The delimitation zones between the layers can be seen as well, due to the presence of fine films of titanium oxides and due to some layer detachments.

If compare the precursor sample with ARB-16 layers sample, the analysis of SEM images come to confirm the above conclusions of the XRD analysis according the idea that ARB process is proper for ultra-fine graining of the structure since it was obtained a highly fine nanometric structure, with average dimension of about 19 nm.

3.2. Corrosion behavior in Ringer solution

3.2.1. Linear polarization measurements

The potentiodynamic linear polarization curves, Tafel representations (some examples are presented in Fig. 6) furnished the main corrosion parameters (Table 2).
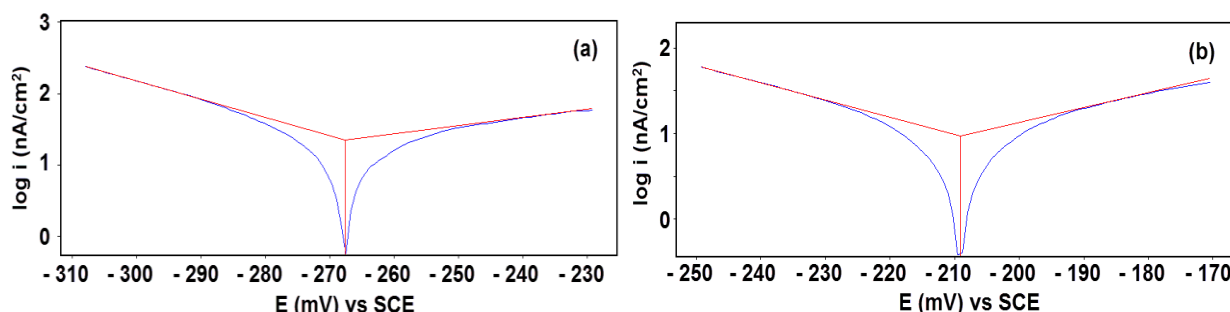

Figure 6. Tafel plots for Ti-25Ta-25Nb alloy obtained in Ringer solution at 37°C: a) ARB precursor state; b) ARB 16 layers processed state.

Table 2. Main corrosion parameters for Ti-25Ta-25Nb alloy in as-cast state and in ARB processed states (precursor, 8 and 16 layers) in Ringer solution at 37°C.

Alloy state	E_{corr} (mV)	i_{corr} (nA/cm^2)	V_{corr} (μm/Y)	Resistance class	R_p (MΩ cm^2)	β_a (mV/dec)	B_c (mV/dec)
As-cast	-280	52	0.460	PS[a]	0.990	137	-114
ARB precursor	-266	28	0.339	PS	1.050	149	-116
ARB 8 layers	-245	11	0.102	PS	1.120	150	-113
ARB 16 layers	-210	8	0.071	PS	1.240	148	-115

[a]PS – Perfect Stable

As can be seen from Table 2 data, corrosion potentials, E_{corr} are nobler for ARB processed alloy, (the noblest E_{corr} for alloy in ARB 16 layers processed state) and ennobled with the number of ARB cycles as result of the favorable effect of the ARB processing; values of the corrosion current densities, i_{corr} and of corrosion rates, V_{corr} are lower for ARB processed alloy than that of as-cast alloy

and decrease with the increase of the number of layers, confirming more protective passive films; polarization resistances, R_p have higher values for ARB processed alloy (>1 MΩ cm^2), suggesting the improvement of protective capacity of the passive oxide layer [34, 35] existing on the processed alloy surface. The values of the anodic β_a Tafel slopes are higher than those of the cathodic β_c Tafel slopes, indicating the anodic control of the corrosion process, i.e., the existence of the passive layer [36]; on the other part, the values of the cathodic β_c Tafel slopes around of -115 mV/dec. denote that the cathodic reaction is the same, hydrogen reduction [36] and does not depend by the processing route. All corrosion parameters enhanced their values by the increase of the layer stacks, namely, the ARB processing has a positive influence on the alloy corrosion resistance.

3.2.2 Monitoring of open circuit potentials

Fig. 7 presents the time variation of open circuit potentials (E_{oc}) for Ti-25Ta-25Nb alloy in as-cast state and in ARB processed states (precursor, 8 and 16 layers) during 1500 immersion in Ringer solution at 37°C. Open circuit potentials for all states of the alloy shifted in the noble direction, showing the growth of the passive films [34, 35] and their barrier action against the metal dissolution; after about 900 hours of immersion for ARB processed alloy and about 1200 hours for as-cast alloy, these potentials tend at a constant level, i.e., the passive films became more stable [37, 38]. Therefore, the increase of the number of ARB cycles conducted to the thickening and stability in time of the alloy passive film.
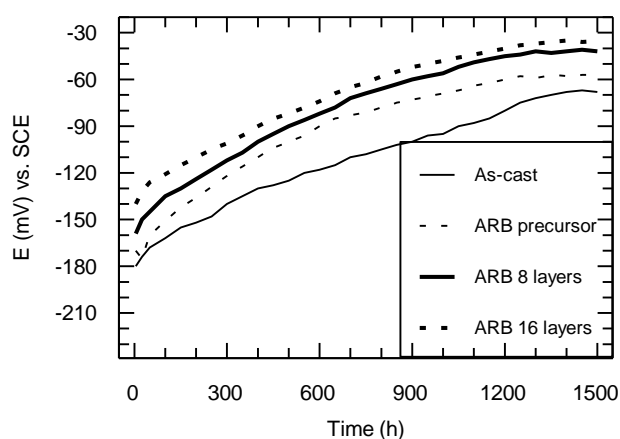

Figure 7. Time monitoring of open circuit potentials for Ti-25Ta-25Nb alloy in: as-cast state, ARB precursor state and in ARB processed states (8 and 16 layers) during immersion in Ringer solution at 37°C.

Fig. 8 illustrates histograms regarding the distribution and frequency of the E_{oc} values for Ti-25Ta-25Nb alloy in as-cast state and in ARB processed states. From these histograms resulted that the frequency of nobler potentials is higher for ARB processed alloy due to the beneficial effect of the applied treatments.
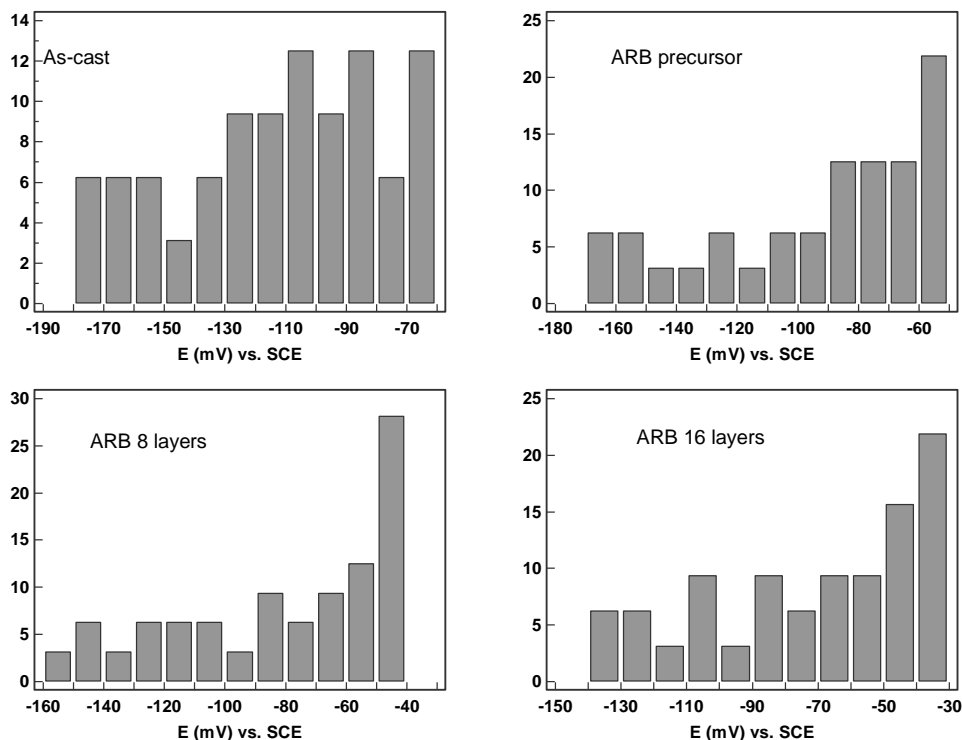
Figure 8. E_{oc} histograms for Ti-25Ta-25Nb alloy in: as-cast state, ARB precursor state and in ARB processed states (8 and 16 layers) during immersion in Ringer solution at 37°C.

Figure 9. E_{oc} scatter diagrams with regression curves for Ti-25Ta-25Nb alloy in: as-cast state, ARB precursor state and in ARB processed states (8 and 16 layers) during immersion in Ringer solution at 37°C.
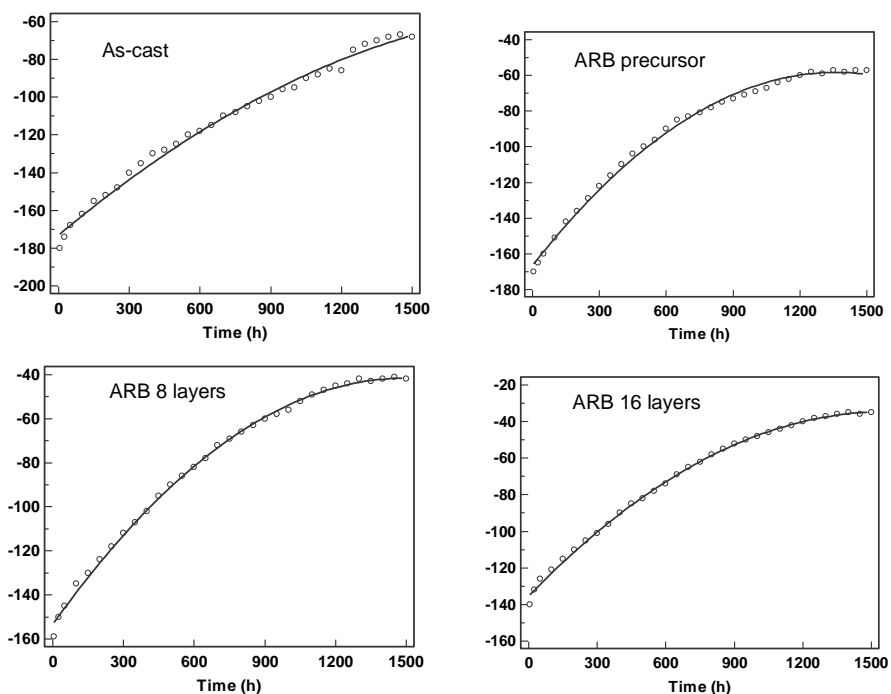
Table 3. Regression equations and determination coefficients (D) for Ti-25Ta-25Nb alloy in: as-cast state, ARB precursor state and in ARB processed states (8 and 16 layers) during immersion in Ringer solution at 37^oC.

Alloy state	Regression equation	D
As-cast	$y = -173.0026 + 0.1050\,x + -0.00002299\,x^2$	0.9923
ARB precursor	$y = -166.3410 + 0.1589\,x + -0.00005840\,x^2$	0.9969
ARB 8 layers	$y = -153.1476 + 0.1496\,x + -0.00005014\,x^2$	0.9980
ARB 16 layers	$y = -135.2114 + 0.1288\,x + -0.00004121\,x^2$	0.9983

Scatter diagrams for 1500 hours of immersion in Ringer solution (Fig. 9) revealed the tendency of the open circuit potentials to move to more electropositive values in time and to reach a constant level, especially for the ARB processed alloy, proving [39] the thickness increase of the passive layer as result of the ARB treatments.

The regression procedure was applied to scatter diagrams and the regression equations and determination coefficients (D) were obtained (Table 3). The determination coefficients have very high values (near 1), showing a very good percent of credibility; therefore, it is possible to estimate the values of E_{oc} for longer time periods than experimental one.

4. CONCLUSIONS

Both XRD analysis and SEM images confirmed that ARB process is proper for ultra-fine graining of the structure since, after four distinct ARB cycles, it was obtained a highly fine nanometric structure, with average dimension of about 19 nm. This final nano-crystalline structure, with β-Ti/α"-Ti ratio decreasing by each ARB cycle, can be controlled in function of final necessary mechanical properties of the alloy: for high strength material is necessary to steer the structure towards small coherent crystalline domains and, on the other hand, for a particular desired elastic modulus in a certain interval range is necessary to steer the structure towards a certain phase β-Ti/α"-Ti ratio (β-Ti phase exhibits a low elastic modulus while α"-Ti phase exhibits a higher elastic modulus).

Corrosion potentials are nobler, corrosion rates decrease and polarization resistances have higher values for the ARB processed alloy and these parameters improved their values with the number of cycles, namely, the ARB processing promote the formation of more protective passive film with the more protective capacity on the Ti-25Ta-25Nb alloy surface. The corrosion process at the interface between processed alloy and simulated physiological environment is controlled by the anodic process, namely, by the passive film. Also, the passive film became more stable in time and thickened with the increase of the number of layers.

References

1. M.A.-H.Gepreel and M. Niinomi, *J. Mech. Behav. Biomed. Mater*. 20 (2013) 407
2. M. Geetha, A.K. Singh, R. Asokamani and A.K. Gogia, *Prog. Mater. Sci,* 54 (2009) 397
3. Y. Kelvin, Y. Wang, Y. Zhao, C. Li, G. Wang, Z. Chen, Y. Cao, X. Liao, E.J. Lavernia, R.Z. Valiev, B. Sarrafpour, H. Zoellner and S.P. Ringer, *Mater. Sci. Eng. C* 33 (2013) 3530
4. D. Kent, G. Wang and M. Dargusch, *J. Mech. Behav. Biomed. Mater*. 28 (2013) 15
5. P. Laheurte, F. Prima, A. Eberhardt, T. Gloriant, M. Wary and E. Patoor, *J. Mech. Behav. Biomed. Mater.* 3 (2010) 565
6. E. Vasilescu, P. Drob, D. Raducanu, V.D. Cojocaru, I. Cinca, D. Iordachescu, R. Ion, M. Popa and C. Vasilescu, *J. Mater. Sci.: Mater. Med*. 21 (2010) 1959
7. D. Mareci, R. Chelariu, D.M. Gordin, G. Ungureanu and T. Gloriant, *Acta Biomater.* 5 (2009) 3625
8. E. Vasilescu, P. Drob, C. Vasilescu, S.I. Drob, E. Bertrand, D.M. Gordin and T. Gloriant, *Mater. Corros*. 61 (2010) 947
9. M. Niinomi and M. Nakai, *Int. J. Biomater.*, Article ID 836587, 10 pages
10. Y. Al-Zain, H.Y. Kim, H. Hosoda, T.H. Nam and S. Miyazaki, *Acta Mater.* 58 (2010) 4212
11. H.Y. Kim, Y. Ikehara, J.I. Kim, H. Hosoda and S. Miyazaki, *Acta Mater.* 54 (2006) 2419
12. Z. Lin, L. Wang, X. Xue, W. Lua, J. Qin and D. Zhang, *Mater. Sci. Eng. C* 33 (2013) 4551
13. D.M. Gordin, T. Gloriant, G. Texier, I. Thibon, D. Ansel, J.L. Duval and M.D. Nagel, *J. Mater. Sci.: Mater. Med.* 15 (2004) 885
14. R.Z. Valiev, Y. Estrin, Z. Horita, T.G. Langdon, M.J. Zehetbauer and Y.T. Zhu, *JOM* 58 (2006) 33
15. Y. Wang, J. Zhao, S. Dai, F. Chen, X. Yu and Y. Zhang, *J. Mech. Behav. Biomed. Mater.* 27 (2013) 33
16. S. Yamaguchi, H. Takadama, T. Matsushita, T. Nakamura and T. Kokubo, *J. Mater. Sci.: Mater. Med.* 21 (2010) 439
17. D.M. Gordin, D. Busardo, A. Cimpean, C. Vasilescu, D. Höche, S.I. Drob, V. Mitran, M. Cornen and T. Gloriant, *Mater. Sci. Eng. C* 33 (2013) 4173
18. E. Bertrand, P. Castany and T. Gloriant, *Acta Mater*. 6 (2013) 511
19. E. Bertrand, T. Gloriant, D.M. Gordin, E. Vasilescu, P. Drob, C. Vasilescu and S.I. Drob, *J. Mech. Behav. Biomed. Mater.* 3 (2010) 559
20. A. Cimpean, V. Mitran, C.M. Ciofrangeanu., B. Galateanu., E. Bertrand., D.M. Gordin, D. Iordachescu and T. Gloriant, *Mater. Sci. Eng. C* 32 (2012) 1554
21. K. Cheng, C. Lu, K. Tieu and H. Zhu, *Metal. Mater. Trans. B* 45 (2014) 399
22. I. Cinca, D. Raducanu, A. Nocivin, D.M. Gordin and V.D.Cojocaru, *Kovove Mater*. 51 (2013) 165
23. D. Terada, S. Inoue and N. Tsuji, *J. Mater. Sci*. 42 (2007) 1673
24. V.D. Cojocaru, D. Raducanu, T. Gloriant and I. Cinca, *JOM* 64 (2012) 572
25. M.T. Mathew, C. Nagelli, R. Pourzal, A. Fischer, M.P. Laurent, J.J. Jacobs and M.A. Wimmer, *J. Mech. Behav. Biomed. Mater*. 29 (2014) 199
26. R.M. Abou Shahba, W.A. Ghannem, A. El-Sayed El-Shenavy, A.S.A. Ahmed and S.M. Tantawy, *Int. J. Electrochem. Sci.* 6 (2011) 5499
27. Z. Liu, X. Liu, U. Donatus, G.E. Thompson and P. Skeldon, *Int. J. Electrochem. Sci.* 9 (2014) 3588
28. C.G. Nava-Dino, R.G. Bautista-Magulis, M.A. Neri-Flores, M.V. Orozco-Carmona, S.D. de la Torre, J.G. Gonzalez-Rodriguez, J.G. Cachon-Nava and A. Martinez-Villafane, *Int. J. Electrochem. Sci.* 7 (2012) 4250
29. S. Hanada, N. Masahashi, T.K. Jung, M. Miyake, Y.S. Sato and H. Kokawa, *J. Mech. Behav. Biomed. Mater.* 32 (2014) 310
30. S. Hanada, N. Masahashi, T.-K. Jung, N. Yamada, G. Yamakoand E. Itoi, *J. Mech. Behav. Biomed. Mater*. 30 (2014) 140
31. H. Liu, M. Niinomi, M. Nakai, J. Hieda and K. Cho, *J. Mech. Behav. Biomed. Mater*. 34 (2014) 66

32. J. He, F. Zhou, G. Chang and E.J. Lavernia, *J. Mater. Sci*. 36 (2001) 2955
33. K. Narita, M. Niinomi and M. Nakai, *J. Mech. Behav. Biomed. Mater.* 29 (2014) 393
34. J. Black, *Biological performance of materials: Fundamentals of biocompatibility*, M. Decker Inc.; New York, (1992)
35. D.J. Blackwood, A.W.C. Chua, K.H.W. Seah, R. Thampuran and S.H. Teoh, *Corros. Sci.* 42 (2003) 481
36. D. Jones, Principes and Prevention of Corrosion, second ed., Prentice-Hall Inc., NJ, 1996
37. S.L. Assis, S. Wolynec and I. Costa, *Electrochim. Acta* 5 (2006) 1815
38. S.L. Assis, S. Wolynec and I. Costa, *Mater. Corros*. 59 (2008) 739
39. J.M. Calderon Moreno, E. Vasilescu, P. Drob, P. Osiceanu, C. Vasilescu, S.I. Drob, M. Popa, *Corros. Sci.* 77 (2013) 52